Journal of Power Sources 196 (2011) 999–1005

Contents lists available at ScienceDirect

Journal of Power Sources

journal homepage: www.elsevier.com/locate/jpowsour

$Bi_{0.5}Sr_{0.5}MnO_3$ as cathode material for intermediate-temperature solid oxide fuel cells

Beibei Liu [a], Zhiyi Jiang [a], Bo Ding [a], Fanglin Chen [b], Changrong Xia [a,b,*]

[a] CAS Key Laboratory of Materials for Energy Conversion, Department of Materials Science & Engineering, University of Science & Technology of China, Hefei 230026, Anhui, China
[b] Department of Mechanical Engineering, University of South Carolina, Columbia, SC 29208, USA

ARTICLE INFO

Article history:
Received 1 August 2010
Received in revised form 21 August 2010
Accepted 23 August 2010
Available online 25 September 2010

Keywords:
Cathode
Perovskite
Manganite
Solid oxide fuel cells

ABSTRACT

$Bi_{0.5}Sr_{0.5}MnO_3$ (BSM), a manganite-based perovskite, has been investigated as a new cathode material for intermediate-temperature solid oxide fuel cells (SOFCs). The average thermal-expansion coefficient of BSM is $14 \times 10^{-6}\,K^{-1}$, close to that of the typical electrolyte material. Its electrical conductivity is 82–200 $S\,cm^{-1}$ over the temperature range of 600–800 °C, and the oxygen ionic conductivity is about $2.0 \times 10^{-4}\,S\,cm^{-1}$ at 800 °C. Although the cathodic polarization behavior of BSM is similar to that of lanthanum strontium manganite (LSM), the interfacial polarization resistance of BSM is substantially lower than that of LSM. The cathode polarization resistance of BSM is only 0.4 $\Omega\,cm^2$ at 700 °C and it decreases to 0.17 $\Omega\,cm^2$ when SDC is added to form a BSM–SDC composite cathode. Peak power densities of single cells using a pure BSM cathode and a BSM–SDC composite electrode are 277 and 349 $mW\,cm^2$ at 600 °C, respectively, which are much higher than those obtained with LSM-based cathode. The high electrochemical performance indicates that BSM can be a promising cathode material for intermediate-temperature SOFCs.

1. Introduction

Solid oxide fuel cell (SOFC) is an energy conversion device which can directly convert chemical energy to electrical energy with high efficiency and low to zero emission. Lanthanum strontium manganite (LSM) perovskites are the most investigated and probably the most important cathode materials for SOFCs. At high temperatures, the LSM cathode offers adequate electrochemical performance. However, at reduced temperatures, LSM cathode has low catalytic activity for oxygen reduction reactions in the cathode mainly due to its negligible oxygen ionic conductivity and low oxygen surface exchange coefficient. Various attempts have been made to improve the LSM cathode performance at reduced temperatures, including (1) using composite cathode consisting of LSM and an electrolyte material to increase the number of triple phase boundary (TPB), (2) replacing the B-site Mn with Fe and/or Co to increase the oxygen exchange rate, and (3) replacing the A-site La with various elements to search for highly active cathodes based on manganite perovskites, which are usually more stable in SOFC operation conditions than Co and/or Fe based cathodes.

Various elements have been investigated to replace the A-site La, including lanthanides and Y. Ishihara et al. [1] have replaced A-site of $La_{0.6}Sr_{0.4}MnO_3$ with Ln, where Ln = La, Pr, Nd, Sm, Gd, Yb, and Y. They found that when Ln = Yb and Y, the electrical conductivity is very low. When Ln = Pr, Nd, Sm, and Gd, the electrical conductivity is comparable to that of $La_{0.6}Sr_{0.4}MnO_3$, which is about 100–240 $S\,cm^{-1}$ at 800 °C. The cathode overpotentials at 1000 °C decrease in the order of Y > Yb > La > Gd > Nd > Sm > Pr, indicating that when Ln = Gd, Nd, Sm and Pr, $Ln_{0.6}Sr_{0.4}MnO_3$ exhibits higher performance than that of $La_{0.6}Sr_{0.4}MnO_3$. Sakaki et al. [2] have investigated the reactivity of these perovskites ($Ln_{1-x}Sr_xMnO_3$, Ln = La, Pr, Nd, Sm, and Gd; $0 \le x \le 0.5$) with yttria-stabilized zirconia (YSZ). The formation of the pyrochlore phase, $Ln_2Zr_2O_7$, is suppressed with the decrease of the ionic radius of Ln^{3+}. $Pr_{1-x}Sr_xMnO_3$ and $Nd_{1-x}Sr_xMnO_3$ have shown better compatibility with YSZ than $La_{1-x}Sr_xMnO_3$. The reactivity between $Gd_{1-x}Sr_xMnO_3$ and YSZ are further investigated by Takeda et al. [3]. They found that $Gd_{1-x}Sr_xMnO_3$ showed much better compatibility with YSZ although its electrochemical activity and electrical conductivity were similar to that of $La_{1-x}Sr_xMnO_3$. However, Yoon et al. [4] have reported the formation of $SrZrO_3$ phase for $Gd_{1-x}Sr_xMnO_3$/YSZ systems heated at 1300 °C for 48 h. Therefore, the A-site cation of the perovskite-type oxide containing B-site Mn has a great influence on not only its electrochemical property as

* Corresponding author at: CAS Key Laboratory of Materials for Energy Conversion, Department of Materials Science & Engineering, University of Science & Technology of China, 96 Jinzhai Rd., Hefei 230026, Anhui, China.
Tel.: +86 551 3607475; fax: +86 551 3606689.
E-mail address: xiacr@ustc.edu.cn (C. Xia).

0378-7753/$ – see front matter © 2010 Elsevier B.V. All rights reserved.
doi:10.1016/j.jpowsour.2010.08.057

SOFC cathode but also chemical compatibility with the electrolyte materials. Although Bi is also a trivalent element, Bi replacement to the A-site element has not yet been evaluated as a potential cathode material for SOFCs.

When the A-site element is Bi, a Sr doped $BiMnO_3$ perovskite is formed. Even though the ionic radius of Bi^{3+} (1.24 Å) is almost the same as that of La^{3+} (1.22 Å), due to its different electronic configuration, especially the highly polarizable $6s^2$ lone pair, (Bi,Sr) MnO_3 perovskites have quite different magnetic and electric properties from that of (La,Sr) MnO_3 [5–7]. Yamada et al. [7] have investigated the physical properties of single crystal $Bi_{1-x}Sr_xMnO_3$. When x approaches 0.5, their electrical conductivity at 523 °C is in the range of 100–200 S cm^{-1}, which is sufficient for SOFC cathodes. In addition, previous work has showed that bismuth oxides has positive catalytic effects on oxygen dissociation process [8], which is often the rate limiting step in oxygen reduction reaction at the SOFC cathode. However, its electrochemical properties as SOFC cathodes have not been studied. In this work, $Bi_{0.5}Sr_{0.5}MnO_3$ (BSM) is evaluated as an alternative cathode material for intermediate-temperature (IT)-SOFCs in terms of thermal-expansion coefficient match with the electrolytes, chemical compatibility with the electrolytes, electrical conductivity, and electrochemical activities towards oxygen reduction properties.

2. Experimental

BSM ($Bi_{0.5}Sr_{0.5}MnO_3$) powder was synthesized using a solid-state reaction method with Bi_2O_3, $SrCO_3$ and $MnCO_3$ as the precursors, which were from Sinopharm Chemical Reagent Co. Ltd. and used without any further treatment. Stoichiometric amounts of Bi_2O_3, $SrCO_3$ and $MnCO_3$ to form the nominal composition of $Bi_{0.5}Sr_{0.5}MnO_3$ were mixed, ball-milled and pressed into discs, which were then calcined in air at 750 °C for 12 h. The calcined samples were grinded to powder, dry-pressed into discs, and subsequently sintered at 1050 °C for 12 h. The sintered sample was re-grinded into powder, and then was used as electrode component for electrochemical characterizations. The BSM powder was also pressed to rectangular bars and sintered at 1200 °C for 5 h for the electrical conductivity and thermal-expansion coefficient measurement. The relative density of the sintered BSM bars was higher than 95% of the theoretical density as measured by the Archimedes method.

To investigate the chemical compatibility between BSM and typical electrolyte materials such as samaria doped ceria (SDC) and yttria-stabilized zirconia (YSZ), BSM powder was mixed at 1:1 weight ratio with SDC and YSZ (Tosch, Japan), pressed to discs, and then fired in air at 700, 800, 900, 950, 1000 and 1050 °C for 12 h, respectively. The SDC powder was synthesized using a glycine–nitrate process [9] and summarized below. $(NH_4)_2Ce(NO_3)_6$ and $Sm(NO_3)_3$ were dissolved in distilled water to form a nitrate solution, to which the glycine was added at a glycine to nitrate molar ratio of 0.5. The solution was heated till self-combustion occurred. The powders were fired at 600 °C for 2 h to form SDC with the fluorite phase.

The oxygen ionic conductivity was measured by an ion-blocking method, with a BSM pellet sandwiched with SDC. The tri-layer structure SDC/BSM/SDC was prepared by co-pressing the powders at 300 MPa and then co-firing the green structure at 1100 °C for 5 h. Pt electrodes were deposited symmetrically on SDC by painting Pt paste (Sino-platinum Metals CO., Ltd.) and then firing at 800 °C for 1 h. The oxygen ionic conductivity of BSM was subsequently measured using AC impedance spectroscopy.

BSM based electrodes were prepared by a screen-printing technique with a slurry containing BSM–SDC. BSM powders were mixed with SDC powders at different weight ratio. The BSM–SDC slurry was obtained by mixing the BSM and SDC powders with terpineol and was then screen printed onto the electrolyte substrate and fired at 800 °C for 2 h. Symmetrical cells, three-electrode half cells, and anode-supported single cells were fabricated to investigate the electrochemical performance of BSM electrodes.

The symmetrical cells were constructed with SDC electrolyte as the substrates to measure the interfacial polarization resistance under open circuit conditions. The substrates were prepared by pressing SDC powders and sintered at 1400 °C for 5 h. The obtained SDC electrolyte substrate is 12.2 mm in diameter and 0.7 mm in thickness. BSM and BSM–SDC electrodes were deposited onto both sides of the substrates using the screen-printing technique as described above. The three-electrode half cells were fabricated to study the effect of current on the electrode performance. Pt counter electrode was deposited symmetrically to the BSM working electrode, at the center of the opposite side of the electrolyte. A ring-shaped Pt reference electrode was prepared around the working electrode. The anode-supported single cells with SDC as the electrolytes and Ni–SDC as the anodes were fabricated with a co-pressing and co-firing method [10] to further characterize the electrode performance. Mixed powders of NiO, SDC and starch (48:32:20, wt%) were prepared to form green-substrates, on which SDC powders were added and co-pressed to form a bilayer structure. The bilayers were co-fired at 1250 °C for 5 h to densify the electrolyte layer. Cathodes were prepared by the same process as the symmetrical cells. The three types of electrochemical testing configurations were illustrated elsewhere [11].

The BSM phase structure and the chemical compatibility with SDC and YSZ were evaluated using X-ray diffraction (XRD, Philip X'pert PROS diffractometer). Microstructure was observed by scanning electron microscopy (SEM, JOEL JSM-6390A). Electrochemical measurements of three types of cells were conducted by a Zaher Im6ex electrochemical workstation in the frequency range of 1 MHz to 100 mHz with signal amplitude of 10 mV using four-probe technique.

3. Results and discussion

3.1. Phase structures and chemical compatibility with electrolytes

Fig. 1 shows the high temperature XRD patterns of BSM powders. Tetragonal perovskite structure is formed when BSM is fired at 1050 °C. This is consistent with those reported by Kim [6] and Chiba et al. [12], who have fired the powder at

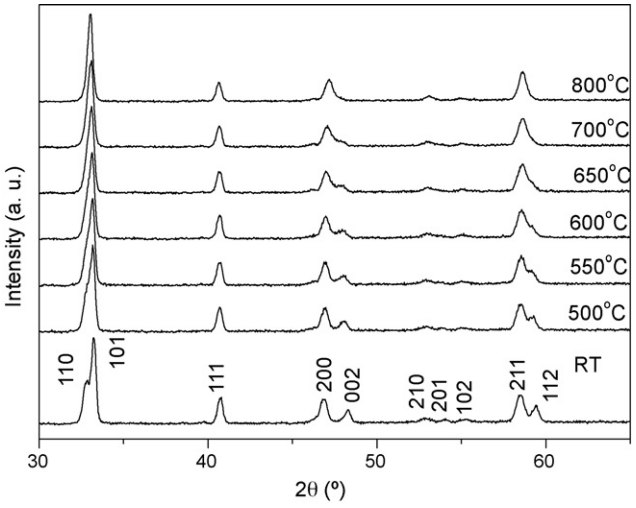

Fig. 1. High temperature XRD patterns of BSM powders, which are prepared with the solid-state reaction method.

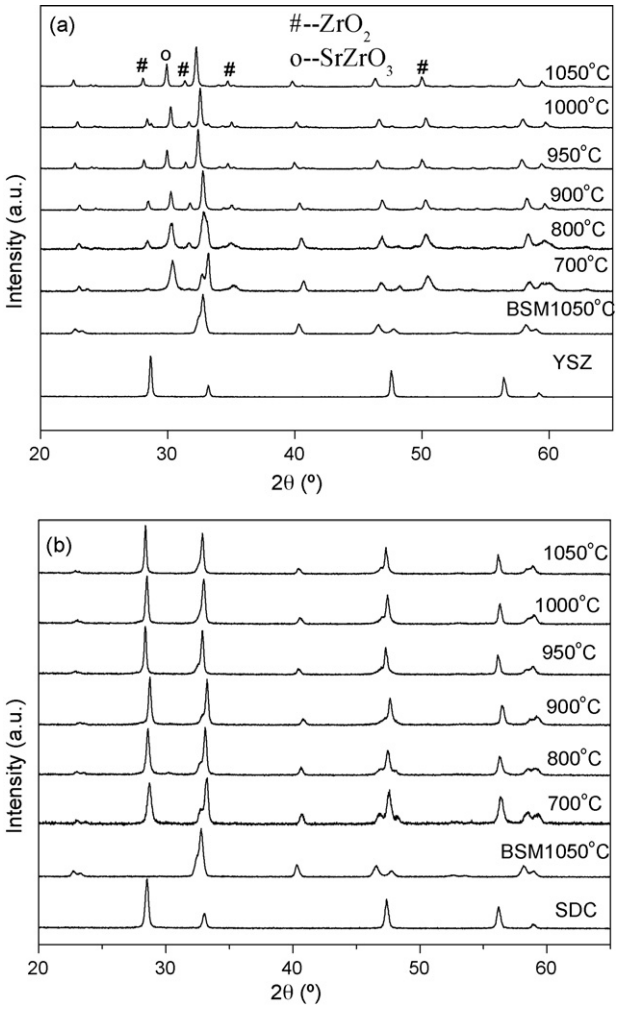

Fig. 2. XRD patterns of (a) BSM and BSM–YSZ composites and (b) BSM–SDC composites fired at various temperatures.

1050 °C and obtained a perovskite BSM. The lattice parameters are $a = b = 3.8722$ Å, $c = 3.7675$ Å. It is also noted that the BSM crystal structure becomes more and more symmetrical with increasing temperature. The obvious evidence is that the separated diffraction peaks of (2 0 0) and (0 2 0), and of (2 1 1) and (1 2 1) planes at room temperature become overlapping at elevated temperatures. Undoped $LaMnO_3$ is orthorhombic at room temperature and shows an orthorhombic/rhombohedral crystallographic transformation at ~600 °C, which is attributed to the oxidation of some Mn^{3+} to Mn^{4+} [13]. The structure transformation of BSM may also be attributed to the oxidation of Mn^{3+} to Mn^{4+}, which reduces the energy tending to produce long-range Jahn–Teller ordering.

Fig. 2a shows the XRD patterns of BSM–YSZ composites fired at various temperatures for 12 h. BSM starts to react with YSZ and forms $SrZrO_3$ even at 700 °C. Thus, BSM is not a good candidate as cathode material for SOFCs based on YSZ electrolytes. Interlayer must be employed between YSZ and BSM when this material is used as the cathode. Fig. 2b shows the XRD patterns for BSM–SDC composites fired at different temperatures. No observable secondary phase is formed between BSM and SDC when the composites are fired at 700–1050 °C, indicating that BSM is chemically compatible with the SDC electrolyte. Therefore, electrochemical characterizations are carried out with the SDC electrolytes, which are often used as the electrolytes for intermediate-temperature SOFCs and as interlayer for YSZ-based SOFCs.

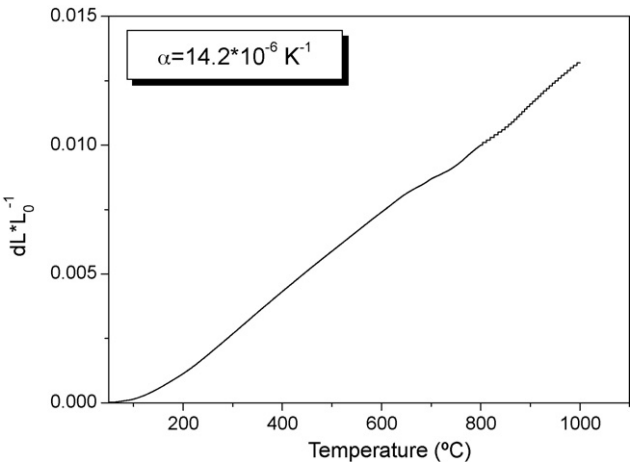

Fig. 3. Thermal-expansion curve of sintered BSM bars.

Shown in Fig. 3 is the thermal-expansion curve. The average thermal-expansion coefficient of BSM is $\sim 14 \times 10^{-6}\,K^{-1}$ between 200 and 800 °C, which is slightly higher than that of LSM ($11.2–12.7 \times 10^{-6}\,K^{-1}$) and SDC ($12 \times 10^{-6}\,K^{-1}$) [13].

3.2. Electronic and oxygen ionic conductivities

The general requirement for a SOFC cathode is high electrical conductivity, e.g., larger than 100 S cm^{-1} at SOFC operating temperatures. Fig. 4 shows the temperature dependence of the electrical conductivity. It is 82–200 S cm^{-1} over the temperature range of 600–800 °C, generally satisfying the requirement for an IT-SOFC cathode and comparable to that of $La_{0.9}Sr_{0.1}MnO_3$, which is 110–120 S cm^{-1} over the same temperature range [14]. The curve of electrical conductivity versus temperature has transitions approximately at 220 and 600 °C, respectively. The transition at 220 °C corresponds to the onset of orbital and charge ordering [5,6]. The change at 600 °C may be caused by the phase change as shown in Fig. 1.

Fig. 5 shows the oxygen ionic conductivity of BSM over the temperature range of 400–750 °C. The conductivity is obtained by measuring the impedance of an electrochemical cell Pt//SDC/BSM/SDC//Pt, in which SDC blocks the electronic conduction [15]. The activation energy is 1.24 eV calculated from the slope of the Arrhenius plot. The oxygen ionic conductivity is about

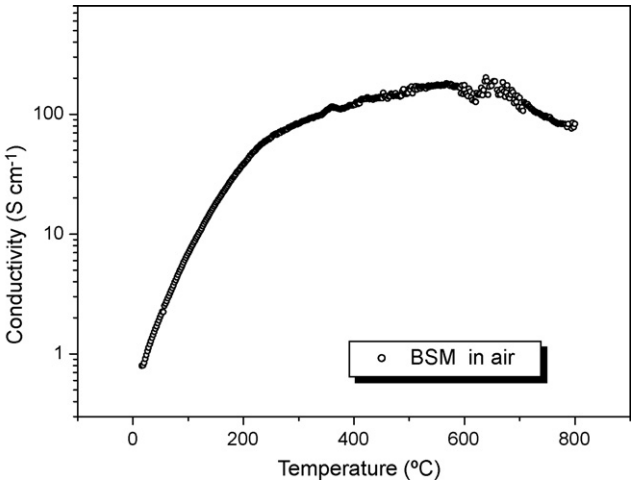

Fig. 4. Electrical conductivity curve of BSM samples measured in air from room temperature to 800 °C.

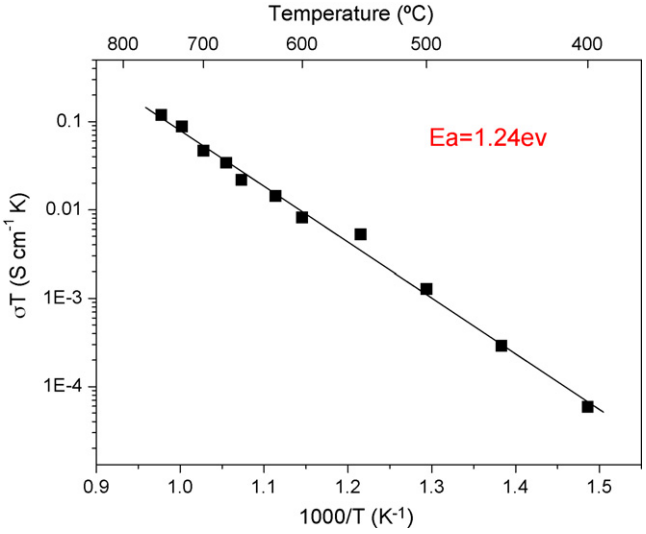

Fig. 5. Oxygen ionic conductivity of BSM over the temperature range of 400–750 °C.

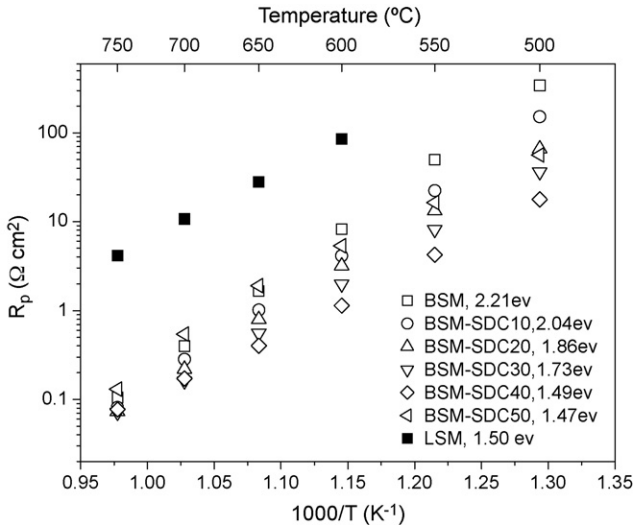

Fig. 6. Interfacial polarization resistance (R_p) over 500–750 °C for BSM and BSM–SDC composite electrodes. The LSM electrode is also listed for comparison.

2.0×10^{-4} S cm^{-1} at 800 °C. It is reported that the oxygen ionic conductivity of $La_{0.65}Sr_{0.35}MnO_3$ at 800 °C measured by Hebb–Wagner technique is 1.7×10^{-4} S cm^{-1} [16] while that of $La_{0.9}Sr_{0.1}MnO_3$ is only 5.9×10^{-8} S cm^{-1} [17]. The oxygen ion conductivity of BSM is higher than that of $La_{0.8}Sr_{0.2}MnO_3$ [18], which is often used as SOFC cathodes. BSM with higher oxygen ion conductivity may have better electrochemical performance than LSM.

3.3. Electrochemical performance under open circuit conditions

Fig. 6 shows the interfacial polarization resistance (R_p) of BSM and BSM–SDC composite electrodes on SDC electrolytes over the temperature of 500–750 °C. R_p is measured with symmetrical cell under open circuit conditions. Thus, R_p is half of the difference between the real axis intercepts of the impedance arcs. R_p for a pure LSM cathode is shown in Fig. 6 for comparison. R_p of a pure BSM cathode is far smaller than that of LSM. For example, at 700 °C, R_p of LSM is 10.67 Ω cm^2, a typical value for pure LSM electrodes [11], while R_p for BSM at the same temperature is only 0.40 Ω cm^2, which is comparable to that of LSCF electrode [19]. Therefore, BSM exhibits much higher electrochemical performance than LSM although they are both Mn-based perovskites. The apparent activation energy (Ea) for the interfacial polarization resistance is also shown in Fig. 6. Ea of the pure BSM electrode is 2.21 eV, which is higher than those reported for LSM cathodes. High Ea value is usually related to the surface processes such as dissociative adsorption and surface diffusion of oxygen species [20]. Therefore, the surface-related processes might determine the oxygen reduction at the BSM electrode.

To improve the electrochemical performance, SDC is added to BSM to form BSM–SDC composite electrodes. The results are also shown in Fig. 6, in which BSM–SDC30 means that the weight percent of SDC is 30%. It can be seen that R_p decreases as the content of SDC increases. The BSM–SDC40 exhibits the lowest R_p among these electrodes, which is only 0.17 Ω cm^2 at 700 °C. However, as SDC content further increases to 50%, R_p increases. Addition of SDC to BSM can produce large amounts of TPBs which reduce the polarization resistance, while too much SDC obstructs the connections between BSM particles, thus decreasing the effective TPBs. The activation energy decreases from 2.21 eV for pure BSM to 1.86 eV for BSM–SDC20, and further to 1.47 eV for BSM–SDC50, indicating the significant electrocatalytic effect of SDC phase on the O_2 reduction processes. This content-dependent relation is very similar to LSM-based composites [20].

Fig. 7 shows the cross-sectional images of a pure BSM electrode and a BSM–SDC40 composite electrode. The size of BSM particles is 2–3 μm (Fig. 7a), while the size of SDC particles is much smaller, ~100 nm (Fig. 7b). Small SDC particles cover the surface of BSM particles, increasing the TPB. According to percolation theory for random packing system, phase with the large particles in a composite system requires high percolation threshold [21], that is, larger volume fraction. Thus, for the BSM–SDC composite electrode, high BSM content is required to maintain high electrode performance.

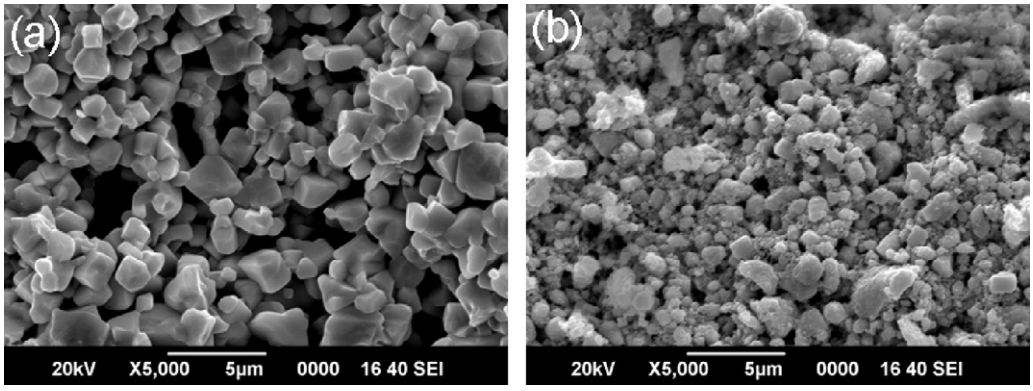

Fig. 7. Cross-sectional images of (a) a pure BSM electrode and (b) a BSM–SDC composite electrode with 40 wt% SDC.

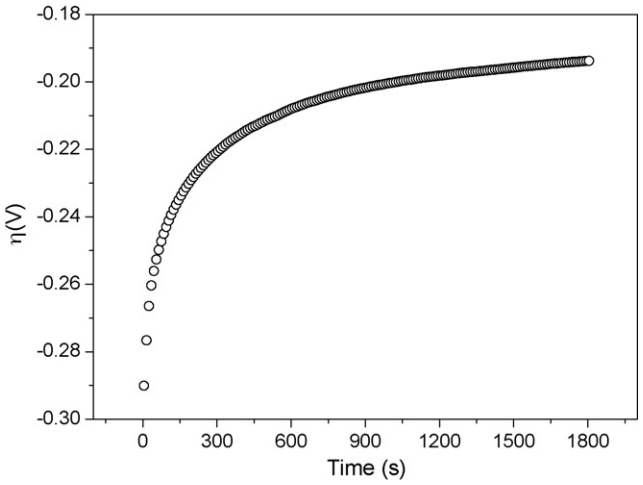

Fig. 8. Cathodic polarization overpotential (η) versus time for a pure BSM electrode under a cathodic current density of 100 mA cm^{-2}. The measurement is conducted at 600 °C using a three-electrode configuration.

3.4. Activation behaviors

A common phenomenon of the LSM-based cathode is the activation effect under fuel cell operation conditions [22]. Since BSM is also a manganite-based perovskite, the behavior of the BSM electrode under cathodic polarization is investigated. Fig. 8 shows the polarization overpotential (η) at 600 °C under a cathodic current density of 100 mA cm^{-2}. The curve shown in Fig. 8 is typical for all the current densities. η is obtained with the following equation:

$$\eta = U_{WR} - iR_{ohm} \quad (1)$$

where U_{WR} is the voltage between the working electrode and the reference electrode, and R_{ohm} is the electrolyte ohmic resistance obtained by electrochemical impedance spectroscopy (EIS) measurement. The overpotential drops quickly in the initial 5 min, but becomes more and more stable with the time, and is stabilized after 25 min. η is 298 mV initially and drops to 189 mV under the 100 mA cm^{-2} in 30 min. The behavior of η as a function of time is similar to that of the LSM electrodes [22].

When the overpotential is stable, EIS is performed under the corresponding current densities. Fig. 9 exhibits the impedance spectra at 600 °C for the 3-electrode cell with the BSM working electrode

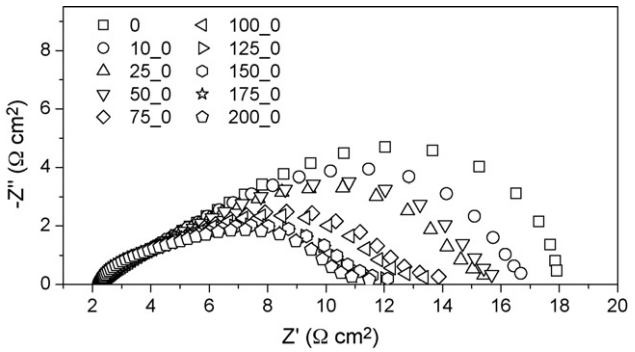

Fig. 10. Impedance spectra at 600 °C under open circuit conditions after polarization of various current densities (numbers represent the current density and "0" represents the measurement conducted under open circuit conditions).

under various cathodic current densities. It clearly shows that R_p decreases with the increase in the applied current density, indicating that the cathodic polarization accelerates the oxygen reduction on the electrode. Under open circuit conditions, R_p is 15.5 Ω cm^2. When the current density is 10 mA cm^{-2}, R_p decreases to 4.7 Ω cm^2. It decreases further to 0.35 Ω cm^2 when the current density is 200 mA cm^{-2}. The shapes of the impedance spectra also change with the current density, indicating that the oxygen reduction processes may alter under cathodic polarization.

Upon completion of the EIS measurement under the applied current density, the current is removed, and another EIS measurement is performed immediately under open circuit conditions. The time interval between the two EIS tests is less than 30 s. Fig. 10 shows the impedance spectra under open circuit conditions following the applied current. The interfacial polarization resistance is larger than the corresponding one obtained under current density, indicating that the effect of cathodic current on cathode polarization is restored when the current is removed. This is also evident with the shape of the impedance spectrum. The spectrum for the fresh sample has a large low frequency arc (Fig. 9, 0 mA cm^{-2}). When a current is applied, the low frequency arc is reduced and shrinks with the magnitude of the applied current density. After the current is removed, the low frequency arc reappeared. The shape change also indicates a relaxation process within the BSM electrode. It should be noted that the effect of polarization is not completely eliminated during the time scale for the EIS measurement, as demonstrated by the fact that under open circuit conditions the electrode polariza-

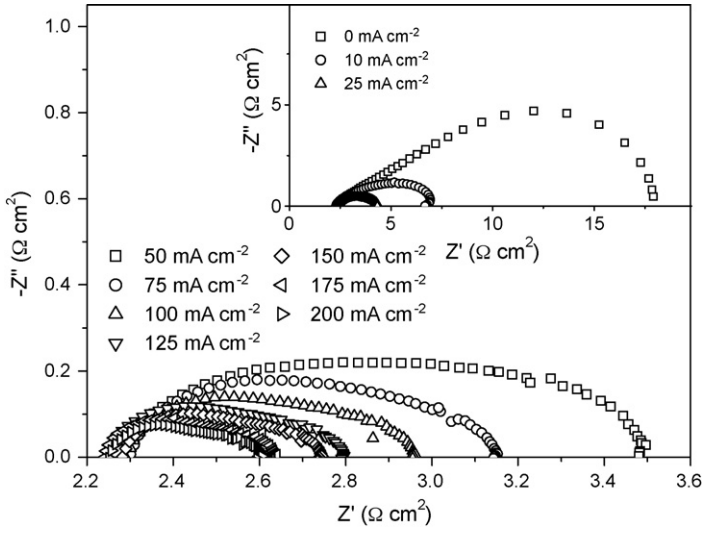

Fig. 9. Impedance spectra for a BSM electrode at 600 °C under various cathodic current densities.

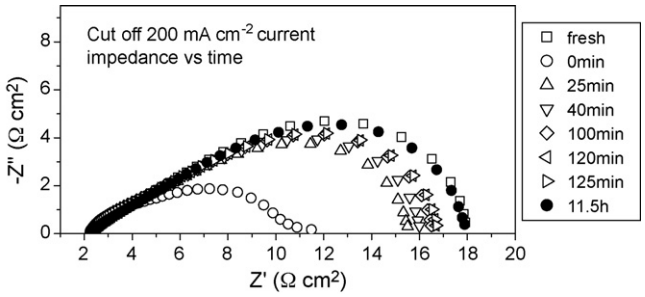

Fig. 11. Relaxation of the electrode impedance spectra measured at 600 °C for a BSM electrode under open circuit conditions after the interruption of 200 mA cm^{-2} current ("fresh" represents no current passing and "0 min" represents after immediately cutting off the current).

tion resistance is still smaller than that of the fresh one. As a general rule, higher current density results in lower interfacial polarization resistance under open circuit conditions, and the obvious difference between the impedance spectra is in the low frequency part.

As motivated by the obvious relaxation phenomenon shown in Fig. 10, the impedance spectra are measured at different times after the 200 mA cm^{-2} current density is interrupted. Fig. 11 shows the electrode impedance evolution with time. At the beginning, impedance changes greatly. The impedance change becomes insignificant subsequently. After 11.5 h, the impedance spectra restores to the same shape as that before the current passage (fresh sample). When the current is interrupted, R_p increases from 0.35 to 9.2 Ω cm^2. After 25 min, R_p increases by about 4 Ω cm^2, but only about 2 Ω cm^2 in the subsequent 11 h. It is also observed that the low frequency part of the impedance spectra changes obviously with time, while high frequency part remains nearly unchanged.

The polarization and EIS measurements indicate that BSM has the similar activation behavior as LSM under cathodic polarization. For LSM electrodes, the origin of the activation is still partly understood. The change of Mn oxidation state (e.g., reduction of Mn^{4+} to Mn^{3+}) and the change of the surface state of the LSM under cathodic polarization are believed to be the main reasons [22–25]. Since both BSM and LSM are manganite-based perovskites, it is reasonable to expect that the cathodic polarization has similar effect on BSM and LSM electrodes. The polarization process indicates that, under cathodic polarization conditions, oxygen vacancies are generated at the electrode/electrolyte interface region by the reduction in manganese ions according to:

$$O^{\times}_{O,BSM} + 2Mn_{Mn,BSM}^{\bullet} + V_{O,SDC}^{\bullet\bullet} + 2e' \rightarrow V_{O,BSM}^{\bullet\bullet} + 2Mn^{\times}_{Mn,BSM} + O^{\times}_{O,SDC} \quad (2)$$

where $Mn_{Mn,BSM}^{\bullet}$ and $Mn^{\times}_{Mn,BSM}$ donate Mn^{4+} and Mn^{3+} ions on BSM lattice, respectively, and $O^{\times}_{O,SDC}$ and $V_{O,SDC}^{\bullet\bullet}$ are the O^{2-} ions and oxygen vacancies on SDC lattice sites, respectively. Oxygen vacancies formed at the BSM/SDC interface region would propagate and extend the reactive sites for the O_2 reduction and thus decrease the polarization resistance. In addition, as the cathodic current density increases, more oxygen vacancies are formed, leading to further reduction of polarization resistance (Fig. 9).

However, the information provided by Figs. 10 and 11 cannot be simply considered to be the reversible process of Eq. (2) because the oxygen diffusion coefficient is usually fast enough to make the polarization resistance recovered to the original condition immediately after switching off the cathodic current. In the present study, the A-site Sr content in perovskite BSM is as high as 50%, higher than that of Sr in LSM. Thus, Sr enrichment on the BSM surface is reasonably anticipated. For the O_2 reduction on the BSM electrode, the SrO originally enriched or segregated on the BSM surface could occupy the active sites and thus inhibit the surface dissociation and

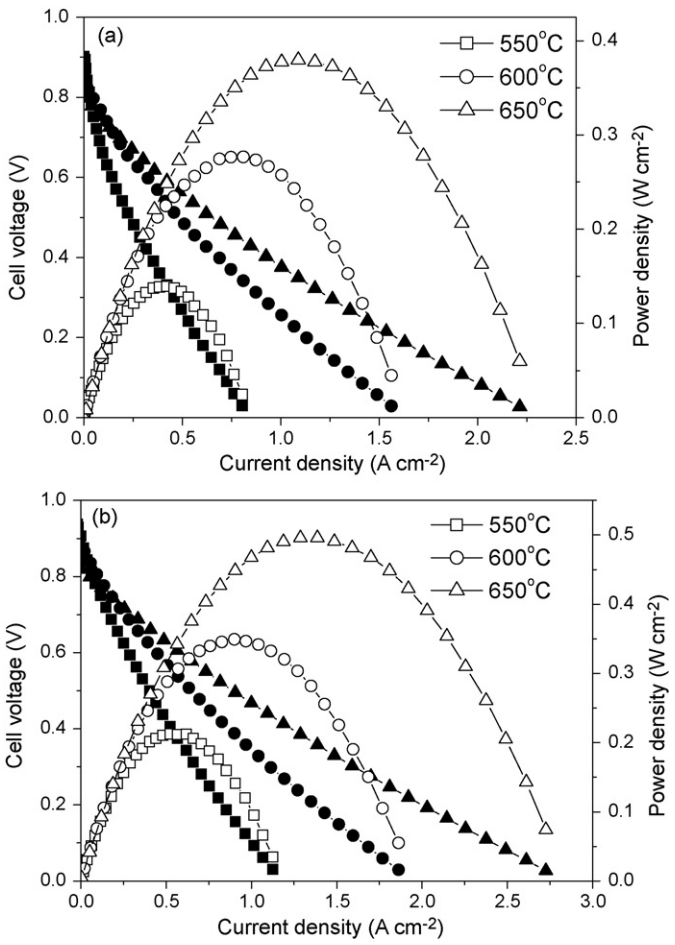

Fig. 12. Performances of single cells (a) with a BSM cathode and (b) with a BSM–SDC composite cathode.

diffusion process. Therefore, the initial significant reduction in the polarization resistance is most likely due to the incorporation of SrO into the BSM perovskite structure under the cathodic current passing treatment:

$$2SrO \rightarrow 2Sr'_{Bi,BSM} + 2O^{\times}_{O,BSM} + V_{O,BSM}^{\bullet\bullet} \quad (3)$$

This indicates that the activation of O_2 reduction reaction on BSM may be limited by two processes: the removal of SrO species and the formation of oxygen vacancies. After the interruption of the cathodic current, the relaxation of the electrode polarization behavior under open circuit conditions is also governed by two steps: the disappearance of oxygen vacancies and the segregation of SrO. The rapid relaxation of impedance spectra measured immediately after the current interruption may reflect the former process. The large time scale (11.5 h) for the impedance spectra to evolve to the original state indicates the presence of the latter process for SrO segregation. When the cathodic current is interrupted, SrO re-segregated on the BSM surface, and this process is accompanied by the Sr^{2+} cation diffusion. Since the cation diffusion coefficient in the perovskite structure is at least three or four orders of magnitude lower than that of oxygen vacancy at the same temperature and oxygen partial pressure [26], a large time scale needs to complete this process. Consequently, the relaxation of the impedance spectra to its original requires 11.5 h (shown in Fig. 11). Both processes change the surface state of BSM, leading to the changes of impedance with time and current densities. The change is dominated by the low frequency parts of the impedance spectra (Figs. 9 and 10), which reflect the surface processes of the oxygen reduction [27].

3.5. Performance of single cells with BSM cathodes

Fig. 12 shows the performances of single cells with BSM and BSM–SDC composite as the cathodes. The electrolyte is SDC with a thickness of about 50 μm and the anode is Ni–SDC. The fuel is humidified hydrogen (~3% H_2O) and ambient air is used as the oxidant. The peak power densities of a single cell using a pure BSM cathode are 133, 277, and 380 mW cm^{-2} at 550, 600 and 650 °C, respectively, while the peak power density using a pure LSM cathode is only 24 mW cm^{-2} at 600 °C. The peak power densities are improved by using a BSM–SDC composite cathode, which are 212, 349 and 496 mW cm^{-2} at 550, 600 and 650 °C, respectively. Furthermore, the performance of BSM cathode can also be improved by optimizing the microstructure such as reducing the particle size of BSM from 2–3 μm to submicronmeter size.

4. Conclusions

$Bi_{0.5}Sr_{0.5}MnO_3$ has been investigated as a potential cathode for SOFCs. XRD analysis shows that BSM reacts with YSZ electrolytes even at 700 °C, while it is chemically compatible with SDC electrolytes up to 1050 °C. Its thermal-expansion coefficient is $\sim 14 \times 10^{-6}$ K^{-1}, close to that of doped ceria electrolytes. Its electrical conductivity is 82–200 S cm^{-1} in the temperature range of 600–800 °C, suitable as electrode for IT-SOFCs. Its oxygen ion conductivity is higher than that of LSM. Electrochemical measurements demonstrate that the polarization resistance at 700 °C for a BSM cathode is only 0.4 Ω cm^2, much lower than that for LSM. The resistance is substantially reduced by adding SDC to BSM to form a composite electrode. The performance of single cells with BSM as the cathodes is also much higher than that with LSM. While BSM shows much higher electrochemical activity than LSM, it exhibits similar activation behaviors as LSM. BSM has shown to be a promising alternative cathode material for intermediate-temperature SOFCs.

Acknowledgements

We gratefully acknowledge the financial support of the Natural Science Foundation of China (10979046 and 50730002) and the US National Science Foundation (CBET 0967166).

References

[1] T. Ishihara, T. Kudo, H. Matsuda, Y. Takita, Journal of the American Ceramic Society 77 (6) (1994) 1682.
[2] Y. Sakaki, Y. Takeda, A. Kato, N. Imanishi, O. Yamamoto, M. Hattori, M. Iio, Y. Esaki, Solid State Ionics 118 (3–4) (1999) 187.
[3] Y. Takeda, H.Y. Tu, H. Sakaki, S. Watanabe, N. Imanishi, O. Yamamoto, M.B. Phillipps, N.M. Sammes, Journal of the Electrochemical Society 144 (8) (1997) 2810.
[4] H.S. Yoon, S.W. Choi, D. Lee, B.H. Kim, Journal of Power Sources 93 (1–2) (2001) 1.
[5] J.L. Garcia-Munoz, C. Frontera, M.A.G. Aranda, A. Llobet, C. Ritter, Physical Review B 63 (6) (2001) 064415.
[6] B.H. Kim, J.S. Kim, M.S. Kim, C.J. Zhang, K.H. Kim, B.G. Kim, H.C. Kim, Y.W. Park, Physics Letters A 351 (4–5) (2006) 368.
[7] S. Yamada, T. Matsunaga, E. Sugano, H. Sagayama, S. Konno, S. Nishiyama, Y. Watanabe, T.H. Arima, Physical Review B 75 (21) (2007) 214431.
[8] J.C. Boivin, G. Mairesse, Chemistry of Materials 10 (10) (1998) 2870.
[9] R.R. Peng, C.R. Xia, Q.X. Fu, G.Y. Meng, D.K. Peng, Materials Letters 56 (6) (2002) 1043.
[10] C.R. Xia, M.L. Liu, Solid State Ionics, Diffusion and Reactions 144 (3–4) (2001) 249.
[11] Z.Y. Jiang, L. Zhang, K. Feng, C.R. Xia, Journal of Power Sources (2008) 40.
[12] H. Chiba, T. Atou, H. Faqir, M. Kikuchi, Y. Syono, Y. Murakami, D. Shindo, Solid State Ionics 108 (1–4) (1998) 193.
[13] S.P. Jiang, Journal of Materials Science 43 (21) (2008) 6799.
[14] J. Mizusaki, Y. Yonemura, H. Kamata, K. Ohyama, N. Mori, H. Takai, H. Tagawa, M. Dokiya, K. Naraya, T. Sasamoto, H. Inaba, T. Hashimoto, Solid State Ionics 132 (3–4) (2000) 167.
[15] C.C. Chen, M.M. Nasrallah, H.U. Anderson, Journal of the Electrochemical Society 142 (2) (1995) 491.
[16] H. Ullmann, N. Trofimenko, F. Tietz, D. Stover, A. Ahmad-Khanlou, Solid State Ionics 138 (1–2) (2000) 79.
[17] A. Endo, M. Ihara, H. Komiyama, K. Yamada, Solid State Ionics 86–88 (1996) 1191.
[18] I. Yasuda, K. Ogasawara, M. Hishinuma, T. Kawada, M. Dokiya, Solid State Ionics 86–88 (1996) 1197.
[19] E.P. Murray, M.J. Sever, S.A. Barnett, Solid State Ionics 148 (1–2) (2002) 27.
[20] S.P. Jiang, W. Wang, Journal of the Electrochemical Society 152 (7) (2005) A1398.
[21] X.J. Chen, S.H. Chan, K.A. Khor, Electrochimica Acta 49 (11) (2004) 1851.
[22] S.P. Jiang, Journal of Solid State Electrochemistry 11 (1) (2006) 93.
[23] S.P. Jiang, J.G. Love, Solid State Ionics 138 (3–4) (2001) 183.
[24] S.P. Jiang, J.G. Love, Solid State Ionics 158 (1–2) (2003) 45.
[25] X.J. Chen, K.A. Khor, S.H. Chan, Solid State Ionics 167 (3–4) (2004) 379.
[26] R.A. De Souza, M.S. Islam, E. Ivers-Tiffee, Journal of Materials Chemistry 9 (7) (1999) 1621.
[27] M.J. Jorgensen, M. Mogensen, Journal of the Electrochemical Society 148 (5) (2001) A433.